INTERNATIONAL JOURNAL FOR NUMERICAL METHODS IN ENGINEERING
Int. J. Numer. Meth. Engng 2003; **57**:1283–1298 (DOI: 10.1002/nme.727)

Variational multiscale methods to embed the macromechanical continuum formulation with fine-scale strain gradient theories

K. Garikipati*,†

Department of Mechanical Engineering, University of Michigan, Ann Arbor, Michigan 48109, U.S.A.

SUMMARY

A variational basis is presented to link fine-scale theories of material behaviour with the classical, macromechanical continuum theory. The approach is based on the weak form of the linear momentum balance equations, and a separation of the weighting function and displacement fields into coarse and fine-scale components. Coarse and fine-scale weak forms are defined. The latter is used to introduce a strain gradient theory that operates at finer scales of deformation. Attention is focused upon applications requiring the enhanced physical accuracy of the fine-scale strain gradient theory, without the computational cost of discretization that spans the range from coarse to fine scales. A variationally consistent method is developed to embed the fine-scale strain gradient theory in the macromechanical formulation. The embedding is achieved by eliminating the fine-scale displacement field from the problem. Two examples demonstrate the numerical efficiency of the method, while retaining physical and mathematical properties of the fine-scale strain gradient theory. Copyright © 2003 John Wiley & Sons, Ltd.

KEY WORDS: variational methods; multiscale problems; strain gradient theories

1. INTRODUCTION

The mechanical behaviour of solid materials demonstrates response over a range of length scales. For polycrystalline solids, macromechanical continuum theories (linear or non-linear elasticity, continuum plasticity, damage degradation, etc.) are sufficient when the deformation phenomena of interest occur at length scales upward of about 10 μm. As deformation phenomena approach the length scales of grains (1 μm and lower in most polycrystalline solids), the interactions between defects and the effects of their elastic fields begin to play increasingly important roles. Restricting attention to polycrystalline solids, it is observed that dislocations, microvoids and microcracks have a pronounced influence upon material response when the deformation varies at the micron and submicron scale. Conventional macroscopic continuum

*Correspondence to: K. Garikipati, Department of Mechanical Engineering, University of Michigan, Ann Arbor, Michigan 48109, U.S.A.
†E-mail: krishna@engin.umich.edu

Contract/grant sponsor: National Science Foundation; contract/grant number: CMS#0087019

Received 1 March 2002
Revised 30 August 2002
Accepted 8 October 2002

theories of inelasticity—such as plasticity or damage—fail at resolving this effect. A treatment of interactions between individual defects is, however, ruled out; their densities are too high to warrant such an approach even at these finer scales. On the other hand, the hardening effects at crack tips, results of nanoindentation tests [1–6], microtorsional and microbending experiments [7, 8], and response in the presence of microvoids, inclusions and microcracks [9] can be explained with notable success by various classes of strain gradient plasticity theories. The observed finite width of shear bands is also represented by these theories since they introduce a length scale to the problem in contrast with classical continuum theories. Several examples of such strain gradient theories have appeared recently [10–17]. A separate approach to incorporating the influence of microstructure is seen in the treatment of configurational microforces [18–21]. Related work [22] treats crystal plasticity in the framework of microforces and encompasses plastic strain gradient effects.

The fine-scale effects of the above models manifest themselves when the deformation varies in the submicron range, thereby inducing sufficiently large strain gradients. In application to boundary-value problems, each class of models outlined above prevails in domains whose dimensions are in the near micron and submicron-range. While using numerical techniques, the finest scales of the discretization must then be in the submicron range. This does not pose a large computational cost if the size of the solid domain over which the boundary-value problem is to be solved is also in the micron range. This would be the case while investigating a crack-tip region, a small region enclosing a micron-sized shear band or the effect of submicron-sized voids in a micron-sized specimen. On the other hand, a wide range of applications require the inclusion of fine-scale physics associated with such microscopic features in *macroscopic* domains. Loading conditions could include wear, fatigue, impact and penetration. They might involve high strain rates and temperatures. Such considerations arise in naval/marine structures, defence and civilian aerospace structures and in industrial settings. These applications place increasingly stringent demands of physical accuracy on material models, thus requiring the incorporation of some of the above microstructural theories. *Yet*, *the overall physical dimensions of the problems remain on the order of* 1–10m *and computational efficiency cannot be forsaken while employing the microstructural theories*. This difficulty would seem to suggest the approach of embedding fine-scale models in macroscopic ones as an alternative. As another option, a microforce theory may be used. In either case the approach should give rise to mathematical models in which deformations at different scales are coupled. Computational efficiency is served if such multiscale models can then be posed solely in terms of the macroscopic coarse-scale deformations. Physical accuracy of the multiscale models will depend upon the fidelity with which microstructural fine-scale physics is represented, and the degree to which it influences the coarse scales.

The approach proposed here is termed the variational multiscale method. The method has previously been applied to the localization of deformation by the author and co-workers [23, 24]. Subsequently, the approach was extended to embed a simple fine-scale traction-separation law in the macromechanical formulation [25, 26]. The method assumes a decomposition of the displacement into coarse and fine-scale components. Within the context of the ideas being proposed here the arguments are as follows:

(i) If one were working with an independent fine-scale law, it would be postulated that the fine-scale displacement component is governed by this law and resolves the microscopic variations of the solution that are absent from the coarse-scale displacement. The

method is variationally based and involves the elimination of fine-scale displacements, resulting in a multiscale model that has microscopic fine scales projected on to the macroscopic coarse scales. The procedure results in an embedding—in the macromechanical formulation—of the fine-scale law that governs the fine-scale physics.

(ii) For a microforce theory, the coupling between scales already exists by way of constitutive laws, micro- and macrobalance laws. In such a case the fine-scale displacement can be exploited to resolve the fine-scale kinematics while the coarse-scale displacement resolves the coarse-scale kinematics. The elimination of the fine-scale displacement results in a multiscale formulation with the microbalance law and fine-scale constitutive law embedded, and the tight coupling of scales being preserved.

The specific fine-scale theory adopted for this article is a phenomenological strain gradient plasticity theory developed by Fleck, Hutchinson and co-workers [11, 27]. It departs from classical plasticity theory when the deformation varies at scales of the order of a micron and below. Under the present view, therefore, it is a fine-scale theory.

The variational basis of the multiscale method presented here results in formulations to which a wide range of discretization techniques can be applied. Specifically, both finite element and meshless methods can be employed. In this article the focus is upon finite-element methods.

The variational multiscale method described here, while related to mathematical homogenization theory, stands apart in that a *constitutive* fine-scale character is assumed of the material. The constitutive laws for fine-scale physics are complemented by a fine-scale balance law. This is to be contrasted with certain (traditional) applications of homogenization theory (see References [28–32] and references therein) where the constitutive model remains that of conventional elasticity while the multiscale character arises from inhomogeneities.

The rest of this paper is organized as follows: The method is developed for the Fleck–Hutchinson strain gradient theory in Section 2. An integration algorithm is presented for this strain gradient plasticity theory in Section 3. The spatial discretization is discussed in Section 4. Two numerical examples appear in Section 5. A summary and long-term scope of this approach are outlined in Section 6.

2. FLECK–HUTCHINSON STRAIN GRADIENT PLASTICITY THEORY AND THE VARIATIONAL MULTISCALE METHOD

The development in this paper assumes small deformations. At the outset a scale separation is introduced on the displacement: $\mathbf{u} = \bar{\mathbf{u}} + \mathbf{u}'$, into coarse- and fine-scale components, respectively. Direct and indicial notation will be used for tensors as appropriate. As discussed in Section 1 the multiscale method will be developed in a variational setting. In this context a displacement weighting function (variation on the displacement), $\mathbf{w}$, arises. It inherits the multiscale decomposition: $\mathbf{w} = \bar{\mathbf{w}} + \mathbf{w}'$. Using the coarse-scale variation $\bar{\mathbf{w}}$, the stress $\boldsymbol{\sigma}$, the body force $\mathbf{f}$, and the traction $\mathbf{t}$, the weak form of the classical (non-gradient) theory is

$$\int_\Omega (\bar{w}_{i,j}\sigma_{ij})\,\mathrm{d}V = \int_\Omega \bar{w}_k f_k\,\mathrm{d}V + \int_{\partial\Omega} \bar{w}_k t_k\,\mathrm{d}S \tag{1}$$

where the domain of integration, Ω, is to be thought of as a macroscopic solid body. The coarse-scale displacement, $\bar{\mathbf{u}}$, and its variation, $\bar{\mathbf{w}}$, are taken to vary on macroscopic scales, say, greater than $10^2\,\mu$m. Thus, Equation (1) can be interpreted as a projection of the macroscopic balance law (stress equilibrium) on these coarse-scale functions. We will refer to this equation as the coarse-scale weak form. The fine-scale fields, $\mathbf{u}'$ and $\mathbf{w}'$, however, vary on much smaller scales: in the micron and submicron range. Thus, if Equation (1) were rewritten with the fine-scale variation, $\mathbf{w}'$, replacing its coarse-scale counterpart, $\bar{\mathbf{w}}$, it would admit the obvious interpretation of projecting the macroscopic balance law on these fine-scale functions. Suppose now that there exists a subdomain, $\Omega' \subset \Omega$, in which it is of interest to take the fine-scale view. Furthermore, let the microstructural nature of Ω' be such that the fine-scale physics discussed in Section 1 comes into play in this subdomain. It would then be of interest to abandon the classical continuum theory in favour of one that can resolve this fine-scale physics. In the present discussion, we would replace the classical theory with the Fleck–Hutchinson strain gradient plasticity theory. On Ω', therefore, we use the following fine-scale weak form, obtained from the Fleck–Hutchinson strain gradient plasticity theory:

$$\int_{\Omega'} (w'_{i,j}\sigma_{ij} + w'_{k,ij}\tau_{ijk})\,\mathrm{d}V = \int_{\Omega'} w'_k f_k\,\mathrm{d}V + \int_{\partial\Omega'} w'_k t_k\,\mathrm{d}S + \int_{\partial\Omega'} (Dw'_k) r_k\,\mathrm{d}S + \sum_i \oint_{C'_i} w'_k p_k\,\mathrm{d}s \tag{2}$$

Observe that the fine-scale displacement variation, $\mathbf{w}'$, is used. In addition to the fields introduced with Equation (1), $\boldsymbol{\tau}$ is the higher-order stress that is conjugate to strain gradients, $\eta_{ijk} = u_{k,ij}$ (further described below) and $\mathbf{r}$ is the couple stress traction. The normal surface gradient operator is $D(\bullet) = \boldsymbol{\nabla}(\bullet)\mathbf{n}$, where $\mathbf{n}$ is the unit normal to the surface in question. The last term on the right-hand side arises when the surface $\partial\Omega'$ has edges that are closed curves, $C'_i,\ i = 1, \ldots, n$. In this setting, $\mathbf{p}$ represents a line load. On comparing Equation (2) with the standard weak form for the classical (non-gradient) theory (see Equation (1)), the difference lies in the second term on the left-hand side and the last two terms on the right. The strain gradient, $\boldsymbol{\eta}$, its conjugate higher-order stress, $\boldsymbol{\tau}$, the couple stress traction, $\mathbf{r}$ and the line load, $\mathbf{p}$, are viewed as fine-scale quantities. This is reasonable, since they appear only with the fine-scale strain gradient plasticity theory and their influence diminishes if the deformation varies at larger scales. Further details and background [11] are omitted here; instead, attention is turned toward the variational multiscale approach for this theory.

2.1. *Embedding the fine-scale strain gradient theory*

Given the two weak forms, we consider the following set of constitutive relations for σ_{ij} and τ_{ijk}:

$$\begin{aligned} &\sigma_{ij} = C_{ijkl}\ \varepsilon^{\mathrm{e}}_{kl}, \quad \tau_{ijk} = A_{ijklmn}\eta^{\mathrm{e}}_{lmn} \\ &\varepsilon_{kl} = \varepsilon^{\mathrm{e}}_{kl} + \varepsilon^{\mathrm{p}}_{kl}, \quad \eta_{lmn} = \eta^{\mathrm{e}}_{lmn} + \eta^{\mathrm{p}}_{lmn} \\ &f(\boldsymbol{\sigma}, \boldsymbol{\tau}) \leqslant 0, \quad \dot{\boldsymbol{\varepsilon}}^{\mathrm{p}} = \lambda \frac{\partial f}{\partial \boldsymbol{\sigma}}, \quad \dot{\eta}^{\mathrm{p}} = \lambda \frac{\partial f}{\partial \boldsymbol{\tau}} \end{aligned} \tag{3}$$

In Equation (3), $\varepsilon^{\mathrm{e}}_{kl}$ and η^{e}_{lmn} are the elastic strain and strain gradient, respectively. The usual fourth-order elasticity tensor is denoted C_{ijkl}, and is given by $C_{ijkl} = \kappa\delta_{ij}\delta_{kl} + \mu(\delta_{ik}\delta_{jl} + \delta_{il}\delta_{jk} - \frac{2}{3}\delta_{ij}\delta_{kl})$, where κ and μ are, respectively, the bulk and shear modulus. The tensor A_{ijklmn} is of sixth order; a material constant, with dimensions of stress$\times$length^2, relating the higher-order stress, τ_{ijk} and elastic strain gradient, η^{e}_{lmn}. Wei and Hutchinson use $A_{ijklmn} = 2E\sum_{\mathrm{I}=1}^{4} L_{\mathrm{I}}^2 T^{(\mathrm{I})}_{ijklmn}$, where E is the Young's modulus, L_{I} is a material length scale and $T^{(\mathrm{I})}_{ijklmn}$, $I = 1,\ldots,4$ are orthogonal projection tensors. A strain gradient *flow theory* of plasticity is also assumed by these authors [27]. The third line of Equation (3) shows the yield criterion and the associative flow rules for rates of plastic strain, $\dot{\boldsymbol{\varepsilon}}^{\mathrm{p}}$, and plastic strain gradient, $\dot{\boldsymbol{\eta}}^{\mathrm{p}}$, respectively.

Up to this stage the decompositions, $\mathbf{u} = \bar{\mathbf{u}} + \mathbf{u}'$ and $\mathbf{w} = \bar{\mathbf{w}} + \mathbf{w}'$ are general. They are made precise by requiring that $\mathbf{u}'$ and $\mathbf{w}'$ vanish outside Ω'. This gives

$$\varepsilon_{ij} := \tfrac{1}{2}(u_{i,j} + u_{j,i}) = \begin{cases} \tfrac{1}{2}(\bar{u}_{i,j} + \bar{u}_{j,i}) & \text{in } \Omega\backslash\Omega' \\ \tfrac{1}{2}(\bar{u}_{i,j} + \bar{u}_{j,i}) + \tfrac{1}{2}(u'_{i,j} + u'_{j,i}) & \text{in } \Omega' \end{cases} \tag{4}$$

$$\eta_{ijk} := u_{k,ij} = \begin{cases} \bar{u}_{k,ij} & \text{in } \Omega\backslash\Omega' \\ \bar{u}_{k,ij} + u'_{k,ij} & \text{in } \Omega' \end{cases} \tag{5}$$

Since the strain gradient theory is applied only over the microstructural subdomain, Ω', it is implied that in $\Omega\backslash\Omega'$, the classical, non-gradient theory provides a sufficiently accurate description of deformation phenomena and material response, and that strain gradients play no role. The kinematics associated with $\boldsymbol{\eta}$ show that the second gradient of the coarse-scale field, $\bar{u}_{k,ij}$, does not necessarily vanish in $\Omega\backslash\Omega'$; however, we will assume that this term plays no role in the material response over this subdomain.

Furthermore, boundary conditions must be imposed upon $\partial\Omega'$. This is achieved by requiring that $\mathbf{u}'$, $\boldsymbol{\nabla}\mathbf{u}'\,\mathbf{n} = \mathbf{0}$ on $\partial\Omega'$. Using (4) and (5), this translates to the requirement that $\mathbf{u}$, $\boldsymbol{\nabla}\mathbf{u}\,\mathbf{n}$ calculated by the strain gradient theory (in Ω') equal $\mathbf{u}$, $\boldsymbol{\nabla}\mathbf{u}\,\mathbf{n}$ calculated by the coarse-scale macromechanical formulation (in $\Omega\backslash\Omega'$) at the fine-scale/coarse-scale interface, $\partial\Omega'$.

The weak form of the fine-scale problem (Equation (2) in this case), will be used to express $\mathbf{u}'$ in terms of the remaining fields in Ω'. The yield condition and flow rule in Equation (3) render the stress, $\boldsymbol{\sigma}$, and higher-order stress, $\boldsymbol{\tau}$, non-linear and history dependent in $\boldsymbol{\varepsilon}$ and $\boldsymbol{\eta}$, respectively. In order to have $\boldsymbol{\varepsilon}$ and $\boldsymbol{\eta}$ appear explicitly in Equation (2), $\boldsymbol{\sigma}$ and $\boldsymbol{\tau}$ must be expanded up to terms of first order in $\delta\boldsymbol{\varepsilon}$ and $\delta\boldsymbol{\eta}$, where $\delta(\bullet)$ denotes an incremental quantity. The following substitutions are made in Equation (2): $\sigma_{ij} = \sigma^0_{ij} + C^{\mathrm{ep}}_{ijkl}\delta\varepsilon_{kl} + B^{\mathrm{ep}}_{ijklm}\delta\eta_{klm}$, $\tau_{ijk} = \tau^0_{ijk} + D^{\mathrm{ep}}_{ijklm}\delta\varepsilon_{lm} + A^{\mathrm{ep}}_{ijklmn}\delta\eta_{lmn}$. The terms σ^0_{ij} and τ^0_{ijk} are of zeroth order while C^{ep}_{ijkl}, B^{ep}_{ijklm}, D^{ep}_{ijklm} and A^{ep}_{ijklmn} are the associated elastoplastic tangents, which upon contraction with $\delta\boldsymbol{\varepsilon}$ and $\delta\boldsymbol{\eta}$ provide the corresponding first-order corrections. This expansion anticipates the cross-coupling between $\boldsymbol{\sigma}$ and $\boldsymbol{\eta}$, and between $\boldsymbol{\tau}$ and $\boldsymbol{\varepsilon}$ that emerges from the Fleck–Hutchinson strain gradient plasticity theory (see Section 3 below). Employing Equations (4) and (5) the following integral relation arises for the *incremental* fine-scale

displacement:

$$\int_{\Omega'} [w'_{i,j}(C^{\mathrm{ep}}_{ijkl}\delta u'_{k,l} + B^{\mathrm{ep}}_{ijklm}\delta u'_{m,kl}) + w'_{k,ij}(D^{\mathrm{ep}}_{ijklm}\delta u'_{l,m} + A^{\mathrm{ep}}_{ijklmn}\delta u'_{n,lm})]\,\mathrm{d}V$$

$$= \int_{\Omega'} w'_k f_k\,\mathrm{d}V + \int_{\partial\Omega'} w'_k t_k\,\mathrm{d}S + \int_{\partial\Omega'} (Dw'_k) r_k\,\mathrm{d}S + \sum_i \oint_{C'_i} w'_k p_k\,\mathrm{d}s - \int_{\Omega'} (w'_{i,j}\sigma^0_{ij} + w'_{k,ij}\tau^0_{ijk})\,\mathrm{d}V$$

$$- \int_{\Omega'} [w'_{i,j}(C^{\mathrm{ep}}_{ijkl}\delta\bar{u}_{k,l} + B^{\mathrm{ep}}_{ijklm}\delta\bar{u}_{m,kl}) + w'_{k,ij}(D^{\mathrm{ep}}_{ijklm}\delta\bar{u}_{l,m} + A^{\mathrm{ep}}_{ijklmn}\delta\bar{u}_{n,lm})]\,\mathrm{d}V \tag{6}$$

Observe that (6) expresses $\delta\mathbf{u}'$ in terms of the coarse-scale field, $\delta\bar{\mathbf{u}}$, and the remaining micro- and macromechanical fields. As is the practice in computational plasticity, an iterative scheme based upon some variant of the Newton–Raphson method is involved in determining the updated fields:

$$\mathbf{u}'^{i+1} = \mathbf{u}'^{i} + \delta\mathbf{u}', \quad \bar{\mathbf{u}}^{i+1} = \bar{\mathbf{u}}^{i} + \delta\bar{\mathbf{u}}$$
$$i = i + 1 \tag{7}$$

until convergence is obtained (see *Remark* (i)). (In Equation (7), i is the iteration number.)

In order to solve Equation (6) for $\delta\mathbf{u}'$, we adopt finite-dimensional approximations of $\mathbf{u}', \bar{\mathbf{u}}$, denoted $\mathbf{u}'^h, \bar{\mathbf{u}}^h$, and the corresponding variations:

$$\mathbf{u}'^h = \sum_A N'^A \boldsymbol{\alpha}_A, \quad \mathbf{w}'^h = \sum_A N'^A \boldsymbol{\theta}_A; \qquad \bar{\mathbf{u}}^h = \sum_A \bar{N}^A \mathbf{d}_A, \quad \bar{\mathbf{w}}^h = \sum_A \bar{N}^A \mathbf{c}_A \tag{8}$$

Substituting (8) in (6), the latter equation can be solved for $\delta\boldsymbol{\alpha}$, and a functional expressing $\delta\mathbf{u}'^h$ in terms of the other fine- and coarse-scale terms is obtained:

$$\delta\mathbf{u}'^h = \mathscr{U}'^h[\delta\bar{\mathbf{u}}^h, \boldsymbol{\sigma}^{h^0}, \boldsymbol{\tau}^{h^0}, \mathbf{C}^{\mathrm{ep}}, \mathbf{B}^{\mathrm{ep}}, \mathbf{A}^{\mathrm{ep}}, \mathbf{D}^{\mathrm{ep}}, \mathbf{t}, \mathbf{r}, \mathbf{p}] \tag{9}$$

Further details on the interpolation functions used in (8), and to determine the discretized form of (9) are presented in Section 4.

Using $\sigma^h_{ij} = \sigma^{h^0}_{ij} + C^{\mathrm{ep}}_{ijkl}[\mathrm{sym}(\delta\bar{u}^h_{k,l}) + \mathrm{sym}(\delta u'^h_{k,l})] + B^{\mathrm{ep}}_{ijklm}[\delta u'^h_{m,kl} + \delta\bar{u}^h_{m,kl}]$ over Ω' in the coarse-scale weak form (1), and substituting the functional (9) for $\delta\mathbf{u}'^h$, the fine-scale field is eliminated from the variational formulation. *This will result in a single weak form for the multi-scale method with the strain gradient theory* (*which governs the fine-scale physics*) *embedded in the classical macromechanical continuum formulation*. The resulting weak form of the variational multiscale method is specific to the chosen model fine-scale physics; in this case, the Fleck–Hutchinson strain gradient plasticity theory.

Since a partial differential equation [the fine-scale weak form, Equation (2)] is solved to obtain $\delta\mathbf{u}'^h = \mathscr{U}'^h[\delta\bar{\mathbf{u}}^h, \boldsymbol{\sigma}^{h^0}, \boldsymbol{\tau}^{h^0}, \mathbf{C}^{\mathrm{ep}}, \mathbf{B}^{\mathrm{ep}}, \mathbf{A}^{\mathrm{ep}}, \mathbf{D}^{\mathrm{ep}}, \mathbf{t}, \mathbf{r}, \mathbf{p}]$, the functional, $\mathscr{U}'^h$, is of integral form. On eliminating $\delta\mathbf{u}'^h$ from the coarse-scale weak form (1), the resulting multiscale weak form is therefore non-local in $\delta\bar{\mathbf{u}}^h$.

Remarks

(i) A typical check for convergence could be specified by requiring that the magnitude of the residual in Equation (6) be less than TOL, where the residual consists of all terms not involving first-order corrections and TOL is a chosen numerical tolerance related to the machine precision. Another check could be $|\delta\bar{\mathbf{u}}^h + \delta\mathbf{u}'^h| < \mathtt{TOL}$.

(ii) The incremental solution scheme outlined above requires integration algorithms for the strain gradient plasticity model. Such an algorithm is discussed in Section 3. The multiscale method and the integration algorithm are both applicable, with minor changes, to the recent improvements proposed in a mechanism-based strain gradient plasticity theory [12, 33], and to the reformulated strain gradient plasticity theory of Fleck and Hutchinson [34].

(iii) The development in this section has been presented as an enhancement of the macroscopic continuum formulation by embedding a fine-scale material law, thus leading to coarse-scale solutions that are more physically accurate. However, it is of some importance to note that the fine-scale solution can also be recovered from the coarse scale: Given the solution $\bar{\mathbf{u}}^h$, use of the functional, $\mathscr{U}'$, gives $\mathbf{u}'^h$. This is a simple post processing step in the numerical setting.

3. AN INTEGRATION ALGORITHM FOR THE STRAIN GRADIENT PLASTICITY THEORY

A phenomenological extension of classical J2-flow theory has been proposed to include the plastic strain gradient and higher order stress tensors [11, 27]. This form has been adopted here. A summary follows; details are available in the papers cited immediately above.

3.1. Flow theory of strain gradient plasticity

The third-order stress tensor, $\boldsymbol{\tau}$ can be decomposed into a hydrostatic term, $\boldsymbol{\tau}_{\mathrm{H}}$, and three deviatoric terms, $\boldsymbol{\tau}_{\mathrm{I}}$, $\mathrm{I} = 1, 2, 3$. These four components are mutually orthogonal. Additionally, three plasticity-related length scales, l_{I}, are identified with the plastic strain gradient, $\boldsymbol{\eta}^{\mathrm{p}}$. Denoting the deviatoric standard stress by $\mathbf{S} := \mathrm{dev}[\boldsymbol{\sigma}]$, and scaled deviatoric higher-order stresses by $\tilde{\boldsymbol{\tau}}_{\mathrm{I}} := \boldsymbol{\tau}_{\mathrm{I}}/l_{\mathrm{I}}$, the generalization of the von Mises yield function with isotropic hardening is

$$\Phi(\boldsymbol{\sigma}, \boldsymbol{\tau}, \mathscr{E}^{\mathrm{p}}) := \sqrt{\frac{3}{2}\,\mathbf{S}:\mathbf{S} + \sum_{\mathrm{I}=1}^{3} \tilde{\boldsymbol{\tau}}_{\mathrm{I}} \dddot{:} \tilde{\boldsymbol{\tau}}_{\mathrm{I}}} - Y(\mathscr{E}^{\mathrm{p}}) \tag{10}$$

Here, $(\bullet)\dddot{:}(\bullet)$ denotes contraction of three indices between the corresponding tensors, and $\mathscr{E}^{\mathrm{p}}$ is the modified equivalent plastic strain given by

$$\dot{\mathscr{E}}^{\mathrm{p}} := \sqrt{\frac{2}{3}\,\dot{\boldsymbol{\varepsilon}}^{\mathrm{p}} : \dot{\boldsymbol{\varepsilon}}^{\mathrm{p}} + \sum_{\mathrm{I}=1}^{3} \dot{\tilde{\boldsymbol{\eta}}}_{\mathrm{I}}^{\mathrm{p}} \dddot{:} \dot{\tilde{\boldsymbol{\eta}}}_{\mathrm{I}}^{\mathrm{p}}} \tag{11}$$

As with the higher-order stress, $\tilde{\boldsymbol{\eta}}^{\mathrm{p}}_{\mathrm{I}} = l_{\mathrm{I}}\boldsymbol{\eta}^{\mathrm{p}}_{\mathrm{I}}$, $\mathrm{I} = 1,2,3$, denotes the three deviatoric plastic strain gradient tensors, that are mutually orthogonal, scaled by l_{I}. Associative flow rules are specified as

$$\boldsymbol{\varepsilon}^{\mathrm{p}} = \gamma \frac{\partial \Phi}{\partial \boldsymbol{\sigma}}, \quad \dot{\tilde{\boldsymbol{\eta}}}^{\mathrm{p}} = \gamma \frac{\partial \Phi}{\partial \tilde{\boldsymbol{\tau}}_{\mathrm{I}}}, \quad \mathrm{I} = 1,2,3 \tag{12}$$

Writing the current yield stress as $Y(\mathscr{E}^{\mathrm{p}}) = Y_0 + K(\mathscr{E}^{\mathrm{p}})$ and defining $q := -K(\mathscr{E}^{\mathrm{p}})$, the evolution law for $\mathscr{E}^{\mathrm{p}}$ can also be cast as an associative flow rule:

$$\dot{\mathscr{E}}^{\mathrm{p}} = \gamma \frac{\partial \Phi}{\partial q} \tag{13}$$

The form of the higher-order elastic modulus, $\mathbf{A}$, introduced in Section 2 gives $\tilde{\tau}_{\mathrm{I}_{ijk}} = (2EL_{\mathrm{I}}^2/l_{\mathrm{I}}^2)\,\tilde{\eta}^{\mathrm{e}}_{\mathrm{I}_{ijk}}$, where E is the Young's modulus and L_{I}, $\mathrm{I} = 1,2,3$, are length scales introduced from dimensional considerations (also see Section 2.1). Wei and Hutchinson require these length scales to be chosen sufficiently small so that they have no influence upon problems where the plastic strain gradients dominate the elastic strain gradients [27].

Given a time-stepping procedure for the initial-boundary value problem, it is assumed that all field values are known at time t_n. With the displacement known at t_{n+1}, the integration algorithm must give $\boldsymbol{\sigma}_{n+1}, \boldsymbol{\tau}_{n+1}, \boldsymbol{\varepsilon}^{\mathrm{e}}_{n+1}, \boldsymbol{\varepsilon}^{\mathrm{p}}_{n+1}, \boldsymbol{\eta}^{\mathrm{e}}_{n+1}, \boldsymbol{\eta}^{\mathrm{p}}_{n+1}$. In the form presented below the integration algorithm is an extension of those for classical plasticity.

3.2. The trial state

The trial or predictor step is based upon the assumption that the plastic flow-dependent variables do not evolve during the step $[t_n, t_{n+1}]$. The total strain and strain gradient are obtained from $\mathbf{u}_{n+1}$ as $\boldsymbol{\varepsilon}_{n+1} := \mathrm{sym}(\partial \mathbf{u}_{n+1}/\partial \mathbf{x})$ and $\boldsymbol{\eta}_{n+1} := \partial^2 \mathbf{u}_{n+1}/\partial \mathbf{x}\partial \mathbf{x}$, respectively. The corresponding trial elastic values are defined as

$$\boldsymbol{\varepsilon}^{\mathrm{e,TR}}_{n+1} := \boldsymbol{\varepsilon}_{n+1} - \boldsymbol{\varepsilon}^{\mathrm{p}}_{n}, \quad \boldsymbol{\eta}^{\mathrm{e,TR}}_{n+1} := \boldsymbol{\eta}_{n+1} - \boldsymbol{\eta}^{\mathrm{p}}_{n} \tag{14}$$

and the corresponding deviatoric trial stresses are

$$\mathbf{S}^{\mathrm{TR}}_{n+1} := 2\mu\, \mathrm{dev}[\boldsymbol{\varepsilon}^{\mathrm{e,TR}}_{n+1}], \quad \tilde{\boldsymbol{\tau}}^{\mathrm{TR}}_{\mathrm{I}_{n+1}} := 2E\frac{L_{\mathrm{I}}^2}{l_{\mathrm{I}}^2}\tilde{\boldsymbol{\eta}}^{\mathrm{e,TR}}_{\mathrm{I}_{n+1}} \tag{15}$$

The trial equivalent plastic strain is defined as

$$\mathscr{E}^{\mathrm{p,TR}}_{n+1} := \mathscr{E}^{\mathrm{p}}_{n} \tag{16}$$

The trial yield condition is examined by evaluating

$$\Phi(\boldsymbol{\sigma}^{\mathrm{TR}}_{n+1}, \boldsymbol{\tau}^{\mathrm{TR}}_{n+1}, \mathscr{E}^{\mathrm{p,TR}}_{n+1}) = \sqrt{\frac{3}{2}\,\mathbf{S}^{\mathrm{TR}}_{n+1} : \mathbf{S}^{\mathrm{TR}}_{n+1} + \sum_{\mathrm{I}=1}^{3} \tilde{\boldsymbol{\tau}}^{\mathrm{TR}}_{\mathrm{I}_{n+1}} \vdots \tilde{\boldsymbol{\tau}}^{\mathrm{TR}}_{\mathrm{I}_{n+1}}} - Y(\mathscr{E}^{\mathrm{p,TR}}_{n+1}) \tag{17}$$

If $\Phi(\boldsymbol{\sigma}^{\mathrm{TR}}_{n+1}, \boldsymbol{\tau}^{\mathrm{TR}}_{n+1}, \mathscr{E}^{\mathrm{p,TR}}_{n+1}) \leqslant 0$, the state obtained by freezing plastic flow in the time interval (t_n, t_{n+1}) is admissible, and the time step is incrementally elastic. All quantities at t_{n+1} are equal to their trial values. The elastoplastic tangents are $\mathbf{C}^{\mathrm{ep}}_{n+1} = \mathbf{C}$ and $\mathbf{A}^{\mathrm{ep}}_{n+1} = \mathbf{A}$.

3.3. The plastic multiplier and update of variables

If $\Phi(\boldsymbol{\sigma}_{n+1}^{\mathrm{TR}}, \boldsymbol{\tau}_{n+1}^{\mathrm{TR}}, \mathscr{E}_{n+1}^{\mathrm{p,TR}}) > 0$, the trial state is inadmissible. Plastic flow must be considered in $[t_n, t_{n+1}]$; i.e. the plastic multiplier, γ in Equations (12) and (13), must be determined. A return mapping algorithm is constructed by adopting the backward Euler integration algorithm for first-order ordinary differential equations. With this choice γ is determined at t_{n+1} and the consistency condition for plastic flow, $\dot{\Phi} = 0$, translates to $\Phi_{n+1} = 0$. The flow rules are written in discretized form as

$$\boldsymbol{\varepsilon}_{n+1}^{\mathrm{p}} = \boldsymbol{\varepsilon}_n^{\mathrm{p}} + \gamma_{n+1}\Delta t \frac{\partial \Phi}{\partial \boldsymbol{\sigma}_{n+1}}, \quad \tilde{\boldsymbol{\eta}}_{\mathrm{I}_{n+1}}^{\mathrm{p}} = \tilde{\boldsymbol{\eta}}_n^{\mathrm{p}} + \gamma_{n+1}\Delta t \frac{\partial \Phi}{\partial \tilde{\boldsymbol{\tau}}_{\mathrm{I}_{n+1}}}, \quad \mathscr{E}_{n+1}^{\mathrm{p}} = \mathscr{E}_n^{\mathrm{p}} + \gamma_{n+1}\Delta t \frac{\partial \Phi}{\partial q_{n+1}} \tag{18}$$

Since the yield function is non-linear in $(\boldsymbol{\sigma}, \tilde{\boldsymbol{\tau}}_{\mathrm{I}}, \mathscr{E}^{\mathrm{p}})$, the condition $\Phi_{n+1} = 0$ is obtained by an iterative procedure—usually the Newton–Raphson method. Denoting the kth iterate of any field at t_{n+1} by $(\bullet)_{n+1}^k$ we have

$$\Phi_{n+1}^{k+1} = \Phi_{n+1}^k + \frac{\partial \Phi^k}{\partial \boldsymbol{\sigma}_{n+1}} : \delta\boldsymbol{\sigma}_{n+1}^k + \sum_{I=1}^{3} \frac{\partial \Phi^k}{\partial \tilde{\boldsymbol{\tau}}_{\mathrm{I}_{n+1}}} \vdots \delta\tilde{\boldsymbol{\tau}}_{\mathrm{I},n+1}^k + \frac{\partial \Phi^k}{\partial q_{n+1}} \delta q_{n+1}^k \tag{19}$$

Observe that Φ is parameterized by $\tilde{\boldsymbol{\tau}}_I$ instead of $\boldsymbol{\tau}_I$ in (19). The deviatoric stress and scaled higher-order stress are

$$\mathbf{S}_{n+1}^k = \mathbf{S}_{n+1}^{\mathrm{TR}} - 2\mu\gamma_{n+1}^k \Delta t \frac{\partial \Phi^k}{\partial \boldsymbol{\sigma}_{n+1}}, \quad \tilde{\boldsymbol{\tau}}_{\mathrm{I}_{n+1}}^k = \tilde{\boldsymbol{\tau}}_{\mathrm{I}_{n+1}}^{\mathrm{TR}} - 2\frac{EL_{\mathrm{I}}^2}{l_{\mathrm{I}}^2}\gamma_{n+1}^k \Delta t \frac{\partial \Phi^k}{\partial \tilde{\boldsymbol{\tau}}_{\mathrm{I}_{n+1}}} \tag{20}$$

Since the hydrostatic stress, $p_{n+1} := \mathrm{tr}[\boldsymbol{\sigma}_{n+1}]$, is independent of plastic strain, we have

$$p_{n+1} = p_{n+1}^{\mathrm{TR}} = \kappa \mathrm{tr}\left[\boldsymbol{\varepsilon}_{n+1}^{\mathrm{e,TR}}\right] \tag{21}$$

From Equations (20) and (21),

$$\underbrace{\left(\mathbb{I} + 2\mu\gamma_{n+1}^k \Delta t \frac{\partial^2 \Phi^k}{\partial \boldsymbol{\sigma} \partial \boldsymbol{\sigma}_{n+1}}\right)}_{\boldsymbol{\Xi}} : \delta\boldsymbol{\sigma}_{n+1}^k = -2\mu\delta\gamma_{n+1}^k \Delta t \frac{\partial \Phi^k}{\partial \boldsymbol{\sigma}_{n+1}}$$

$$\Longrightarrow \delta\boldsymbol{\sigma}_{n+1}^k = -2\mu\delta\gamma_{n+1}^k \Delta t \boldsymbol{\Xi}^{-1} : \frac{\partial \Phi^k}{\partial \boldsymbol{\sigma}_{n+1}} \tag{22}$$

where $\mathbb{I}$ is the fourth-order symmetric identity tensor. Similarly,

$$\underbrace{\left(\mathscr{I} + 2\frac{EL_{\mathrm{I}}^2}{l_{\mathrm{I}}^2}\gamma_{n+1}^k \Delta t \frac{\partial^2 \Phi^k}{\partial \tilde{\boldsymbol{\tau}}_{\mathrm{I}} \partial \tilde{\boldsymbol{\tau}}_{\mathrm{I}_{n+1}}}\right)}_{\mathscr{X}_{\mathrm{I}}} : \delta\tilde{\boldsymbol{\tau}}_{\mathrm{I}_{n+1}}^k = -2\frac{EL_{\mathrm{I}}^2}{l_{\mathrm{I}}^2}\delta\gamma_{n+1}^k \Delta t \frac{\partial \Phi^k}{\partial \tilde{\boldsymbol{\tau}}_{\mathrm{I}_{n+1}}}$$

$$\Longrightarrow \delta\tilde{\boldsymbol{\tau}}_{\mathrm{I}_{n+1}}^k = -2\frac{EL_{\mathrm{I}}^2}{l_{\mathrm{I}}^2}\delta\gamma_{n+1}^k \Delta t \boldsymbol{\chi}_{\mathrm{I}}^{-1} : \frac{\partial \Phi^k}{\partial \tilde{\boldsymbol{\tau}}_{\mathrm{I}_{n+1}}} \tag{23}$$

where $\mathscr{I}$ is a sixth-order identity tensor satisfying $\mathscr{I}_{ijklmn} = \mathscr{I}_{ikjlmn} = \mathscr{I}_{ijklnm}$. The increment δq^k_{n+1} is (see the paragraph preceding (13)):

$$\delta q^k_{n+1} = -K'(\mathscr{E}^{\mathrm{p},k}_{n+1})\delta\gamma^k_{n+1}\Delta t\,\frac{\partial \Phi^k}{\partial q_{n+1}} \tag{24}$$

On substituting the second line of Equations (22) and (23), and Equation (24) in (19), and requiring $\Phi^{k+1}_{n+1} = 0$,

$$\delta\gamma^k_{n+1}\Delta t = \frac{\Phi^k_{n+1}}{\partial\Phi^k/\partial\boldsymbol{\sigma}_{n+1} : 2\mu\,\boldsymbol{\Xi}^{-1} : \partial\Phi^k/\partial\boldsymbol{\sigma}_{n+1} + \sum_{I=1}^{3} \partial\Phi^k/\partial\tilde{\boldsymbol{\tau}}_{\mathrm{I}_{n+1}} \vdots 2\,(EL_1^2/l_1^2)\boldsymbol{\chi}_1{}^{-1} \vdots \partial\Phi^k/\partial\tilde{\boldsymbol{\tau}}_{\mathrm{I}_{n+1}} + K'(\mathscr{E}^{\mathrm{p},k}_{n+1})} \tag{25}$$

The plastic multiplier is updated as $\gamma^{k+1}_{n+1} = \gamma^k_{n+1} + \delta\gamma^k_{n+1}$.

The elastoplastic tangents are obtained as follows:

$$\Delta\boldsymbol{\sigma}_{n+1} = \mathbf{C} : (\Delta\boldsymbol{\varepsilon}_{n+1} - \Delta\boldsymbol{\varepsilon}^{\mathrm{p}}_{n+1}) \tag{26}$$

where

$$\Delta\boldsymbol{\varepsilon}^{\mathrm{p}}_{n+1} = \gamma_{n+1}\Delta t\,\frac{\partial^2\Phi^k}{\partial\boldsymbol{\sigma}\partial\boldsymbol{\sigma}_{n+1}} : \Delta\boldsymbol{\sigma}_{n+1} + \Delta\gamma_{n+1}\Delta t\,\frac{\partial\Phi^k}{\partial\boldsymbol{\sigma}_{n+1}} \tag{27}$$

This yields the relation

$$\Delta\boldsymbol{\sigma}_{n+1} = \mathbb{C}_{n+1} : \left[\Delta\boldsymbol{\varepsilon}_{n+1} - \Delta\gamma_{n+1}\Delta t\,\frac{\partial\Phi^k}{\partial\boldsymbol{\sigma}_{n+1}}\right] \tag{28}$$

where the *algorithmic* modulus is defined as

$$\mathbb{C}_{n+1} = \left[\mathbf{C}^{-1} + \gamma_{n+1}\Delta t\,\frac{\partial^2\Phi}{\partial\boldsymbol{\sigma}\partial\boldsymbol{\sigma}_{n+1}}\right]^{-1} \tag{29}$$

Likewise, for the modified, deviatoric higher-order stresses, we have

$$\Delta\tilde{\boldsymbol{\tau}}_{\mathrm{I}_{n+1}} = \mathbf{A} \vdots (\Delta\tilde{\boldsymbol{\eta}}_{\mathrm{I}_{n+1}} - \Delta\tilde{\boldsymbol{\eta}}^{\mathrm{p}}_{\mathrm{I}_{n+1}}) \tag{30}$$

where

$$\Delta\tilde{\boldsymbol{\eta}}^{\mathrm{p}}_{\mathrm{I}_{n+1}} = \gamma_{n+1}\Delta t\,\frac{\partial^2\Phi}{\partial\tilde{\boldsymbol{\tau}}_{\mathrm{I}}\partial\tilde{\boldsymbol{\tau}}_{\mathrm{I}_{n+1}}} \vdots \Delta\tilde{\boldsymbol{\tau}}_{\mathrm{I}_{n+1}} + \Delta\gamma_{n+1}\Delta t\,\frac{\partial\Phi}{\partial\tilde{\boldsymbol{\tau}}_{\mathrm{I}_{n+1}}} \tag{31}$$

This yields the relation

$$\Delta\tilde{\boldsymbol{\tau}}_{\mathrm{I}_{n+1}} = \mathbb{A}_{n+1} \vdots \left[\Delta\tilde{\boldsymbol{\eta}}_{\mathrm{I},n+1} - \Delta\gamma_{n+1}\Delta t\,\frac{\partial\Phi}{\partial\tilde{\boldsymbol{\tau}}_{\mathrm{I}_{n+1}}}\right] \tag{32}$$

where the *algorithmic* modulus is defined as

$$\mathbb{A}_{n+1} = \left[\mathbf{A}^{-1} + \gamma_{n+1} \Delta t \, \frac{\partial^2 \Phi}{\partial \tilde{\boldsymbol{\tau}}_{\mathrm{I}} \partial \tilde{\boldsymbol{\tau}}_{\mathrm{I}_{n+1}}} \right]^{-1} \tag{33}$$

For the stress-like variable, q, we have

$$\Delta q_{n+1} = -\Delta \gamma_{n+1} \Delta t K'_{n+1} \, \frac{\partial \Phi}{\partial q_{n+1}} \tag{34}$$

Next, the algorithmic consistency condition, $\Delta \Phi(\boldsymbol{\sigma}_{n+1}, \boldsymbol{\tau}_{n+1}, \mathscr{E}^{\mathrm{p}}_{n+1}) = 0$, gives

$$\frac{\partial \Phi}{\partial \boldsymbol{\sigma}} : \Delta \boldsymbol{\sigma}_{n+1} + \sum_{\mathrm{I}=1}^{3} \frac{\partial \Phi}{\partial \tilde{\boldsymbol{\tau}}_{\mathrm{I}}} \vdots \Delta \tilde{\boldsymbol{\tau}}_{\mathrm{I}_{n+1}} + \frac{\partial \Phi}{\partial q} \, \Delta q_{n+1} = 0 \tag{35}$$

On substituting relations (28), (32) and (34) into (35) we have

$$\Delta \gamma_{n+1} \Delta t = \frac{\partial \Phi / \partial \boldsymbol{\sigma}_{n+1} : \mathbb{C}_{n+1} : \Delta \boldsymbol{\varepsilon}_{n+1} + \sum_{\mathrm{I}=1}^{3} \partial \Phi / \partial \tilde{\boldsymbol{\tau}}_{\mathrm{I}_{n+1}} \vdots \mathbb{A}_{n+1} \vdots \Delta \tilde{\boldsymbol{\eta}}_{\mathrm{I}_{n+1}}}{\partial \Phi / \partial \boldsymbol{\sigma}_{n+1} : \mathbb{C}_{n+1} : \partial \Phi / \partial \boldsymbol{\sigma}_{n+1} + \sum_{\mathrm{I}=1}^{3} \partial \Phi / \partial \tilde{\boldsymbol{\tau}}_{\mathrm{I}_{n+1}} \vdots \mathbb{A}_{n+1} \vdots \partial \Phi / \partial \tilde{\boldsymbol{\tau}}_{\mathrm{I}_{n+1}} + K'_{n+1}} \tag{36}$$

Finally, from (28), (32) and (36) we have

$$\mathbf{C}^{\mathrm{ep}}_{n+1} := \frac{\partial \boldsymbol{\sigma}}{\partial \boldsymbol{\varepsilon}_{n+1}} = \mathbb{C}_{n+1} - \mathbb{N}_{n+1} \otimes \mathbb{N}_{n+1} \tag{37}$$

$$\mathbf{B}^{\mathrm{ep}}_{n+1} := \frac{\partial \boldsymbol{\sigma}}{\partial \tilde{\boldsymbol{\eta}}_{\mathrm{I}_{n+1}}} = -\mathbb{N}_{n+1} \otimes \mathbb{M}_{\mathrm{I}_{n+1}} \tag{38}$$

$$\mathbf{D}^{\mathrm{ep}}_{n+1} := \frac{\partial \tilde{\boldsymbol{\tau}}_{\mathrm{I}}}{\partial \boldsymbol{\varepsilon}_{n+1}} = -\mathbb{M}_{\mathrm{I}_{n+1}} \otimes \mathbb{N}_{n+1} \tag{39}$$

$$\mathbf{A}^{\mathrm{ep}}_{n+1} := \frac{\partial \tilde{\boldsymbol{\tau}}_{\mathrm{I}}}{\partial \tilde{\boldsymbol{\eta}}_{\mathrm{I}_{n+1}}} = \mathbb{A}_{n+1} - \mathbb{M}_{\mathrm{I}_{n+1}} \otimes \mathbb{M}_{\mathrm{I}_{n+1}} \tag{40}$$

where

$$\mathbb{N}_{n+1} := \frac{\mathbb{C}_{n+1} : \partial \Phi / \partial \boldsymbol{\sigma}_{n+1}}{\sqrt{\partial \Phi / \partial \boldsymbol{\sigma}_{n+1} : \mathbb{C}_{n+1} : \partial \Phi / \partial \boldsymbol{\sigma}_{n+1} + \sum_{\mathrm{I}=1}^{3} \partial \Phi / \partial \tilde{\boldsymbol{\tau}}_{\mathrm{I}_{n+1}} \vdots \mathbb{A}_{n+1} \vdots \partial \Phi / \partial \tilde{\boldsymbol{\tau}}_{\mathrm{I}_{n+1}} + K'_{n+1}}} \tag{41}$$

$$\mathbb{M}_{\mathrm{I}_{n+1}} := \frac{\mathbb{A}_{n+1} \vdots \dfrac{\partial \Phi}{\partial \tilde{\boldsymbol{\tau}}_{\mathrm{I}_{n+1}}}}{\sqrt{\partial \Phi / \partial \boldsymbol{\sigma}_{n+1} : \mathbb{C}_{n+1} : \partial \Phi / \partial \boldsymbol{\sigma}_{n+1} + \sum_{\mathrm{I}=1}^{3} \partial \Phi / \partial \tilde{\boldsymbol{\tau}}_{\mathrm{I}_{n+1}} \vdots \mathbb{A}_{n+1} \vdots \partial \Phi / \partial \tilde{\boldsymbol{\tau}}_{\mathrm{I}_{n+1}} + K'_{n+1}}} \tag{42}$$

Attention is drawn to the coupling between second- and third-order tensors under plasticity, evident in the generalized tangent relationships, and anticipated in Section 2.1. The plastic multiplier, γ, is driven by $\boldsymbol{\varepsilon}$ and $\boldsymbol{\eta}$. This leads to a dependence of $\Delta \boldsymbol{\sigma}$ upon $\Delta \tilde{\boldsymbol{\eta}}_{\mathrm{I}}$ and of $\Delta \tilde{\boldsymbol{\tau}}_{\mathrm{I}}$ upon $\Delta \boldsymbol{\varepsilon}$, which is absent under purely elastic deformation.

4. FINITE-ELEMENT DISCRETIZATION

The discretized form of the variational multiscale method hinges upon the fine-scale interpolation functions. A test of consistency must be imposed upon the method in order to restrict the form of N' in (8). For uniform material properties, C_{ijkl} and A_{ijklmn}, uniform stress $\boldsymbol{\sigma}$, vanishing body force and boundary traction, and if further, $L_{\mathrm{I}}/l_{\mathrm{I}} \ll 1$ [11, 27], the incremental fine-scale field in (6) must vanish. This translates to the requirement

$$\int_{\Omega'} w'_{i,j}\,\mathrm{d}V = 0 \tag{43}$$

For the boundary-value problem considered in Section 4, $\Omega' = \Omega_e$ for a particular element e. In this case (43) reduces to

$$\int_{\Omega_e} \boldsymbol{\nabla} N'^{A}\,\mathrm{d}V = 0, \ \forall A \tag{44}$$

This test has been described previously [24] for the variational multiscale method applied to strain localization problems.

For the boundary value problem solved in Section 5, the fine scale, strain gradient theory is applied over Ω', which contains a narrow, materially inhomogeneous region of width $2k < \mathrm{meas}(\Omega')$. Additionally, $\mathrm{meas}(\Omega') = \mathrm{meas}(\Omega_e) = h$, and the length scales $l_1, l_2, l_3 = l$ for the boundary-value problem. In terms of the natural co-ordinate, $\xi \in [-1, 1]$, the fine-scale interpolation function is:

$$N'(\xi) = \begin{cases} \frac{1}{4}(1 - (\frac{h}{2l})^3)\xi^3 - \frac{3}{4}(1 - \frac{h}{2l})\xi, & |\xi| \leqslant k/h \\ \frac{1}{4}\xi^3 - \frac{3}{4}\xi - \frac{1}{2}, & -1 \leqslant \xi \leqslant -k/h \\ \frac{1}{4}\xi^3 - \frac{3}{4}\xi + \frac{1}{2}, & k/h \leqslant \xi \leqslant 1 \end{cases} \tag{45}$$

(see Figure 1). The fine-scale interpolation function, thus defined, satisfies (44), and determines functional (9)–(6). The coarse-scale shape functions, $\bar{N}$ are the usual linear Lagrange polynomials.

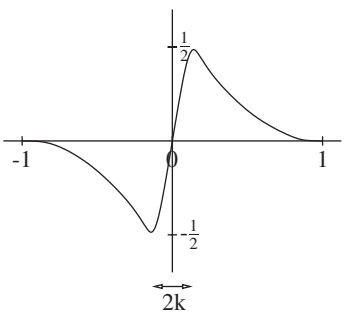

Figure 1. Fine-scale interpolation function, N'.

Remark

(iv) The strain gradient plasticity theory is of fourth order. Therefore, higher-order inter-element continuity requirements must be imposed upon the numerical scheme. This has been attempted previously via a combination of $\mathscr{C}^1$-continuous interpolations and mixed methods [35]. Success has been mixed, at best, and numerical analysis of these methods is also absent. The discretization for the boundary-value problem solved in Section 4, and for which a fine-scale interpolation function has been presented in this section, circumvents this issue by using $\Omega' = \Omega_e$ for some element. Thereby, inter-element continuity is avoided, since N' in (45) is a $\mathscr{C}^\infty$ function. The author and co-workers have recently developed a class of continuous/discontinuous Galerkin methods [36] that allows the use of $\mathscr{C}^0$ interpolations for such strain gradient theories. Thus, no new degrees of freedom need be introduced, and numerical efficiency is assured. A complete numerical analysis of the continuous/discontinuous Galerkin methods for the higher-order strain gradient theory has also been presented in that work—an important contribution that was hitherto missing in the literature.

5. NUMERICAL EXAMPLES

To demonstrate the embedding of this strain gradient theory a bimaterial shear layer is considered. We wish to embed, in turn, a soft material and a hard material within a 'matrix'. The strain gradient plasticity theory will be applied to the neighbourhood, Ω', of the embedded layer, in an attempt to better represent the fine-scale physics. The embedded layer is contained in Ω'. The domain and boundary-value problem are shown schematically in Figure 2. The domain is assumed to be infinite in the vertical direction, allowing the problem to be reduced to one dimension. Of interest are the vertical displacement, u_2, the corresponding shear strain, $\varepsilon_{12} = \frac{1}{2}u_{2,1}$, the strain gradient, $u_{2,11}$, and the shear stress, σ_{12}. Also relevant is the higher-order stress τ_{112}.

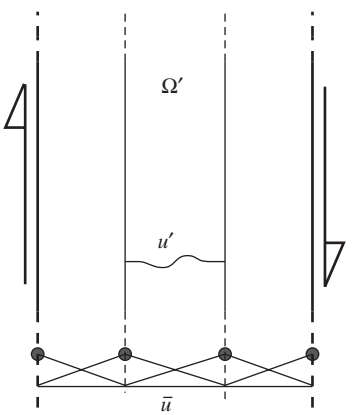

Figure 2. Schematic of shear layer with the fine-scale region.

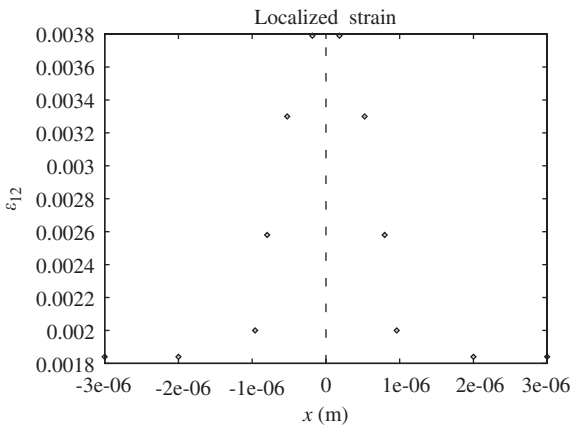

Figure 3. Localized strain in a softening fine-scale region.

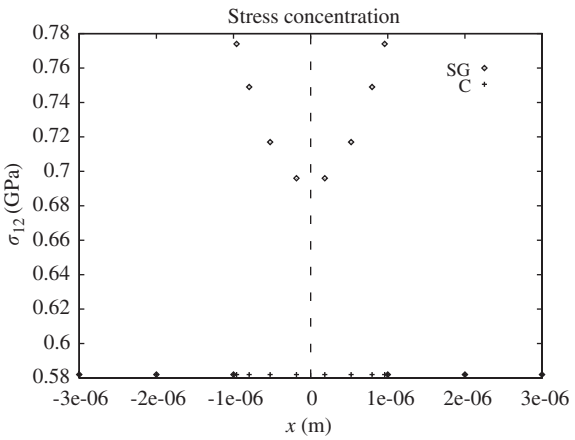

Figure 4. Stress concentrations at the edge of a hardening fine-scale region.

The embedded layer in each case is 2×10^{-6} m in width. The material length scales $L_1, L_2, L_3, l_1, l_2, l_3$ which enter the constitutive law for the strain gradient plasticity theory have each been specified to be 1×10^{-6} m.

Figure 3 is a plot of the strain when the embedded layer is subject to plastic softening. Localization of strain is observed within the softening layer. The width of the localized band is related to the material length scale. In this example it is $\approx 2\times10^{-6}$ m in width.

The shear stress distribution for a hardening embedded layer appears in Figure 4. Attention is drawn to the stress concentrations located at the edges of the hardening layer. It is pointed out that, with a classical (non-gradient) plasticity theory, the shear stress remains constant over the domain. This is shown by the points labelled 'C'. For the strain gradient plasticity theory, however, this is not the case. The equilibrium equation involves the conventional stress $\boldsymbol{\sigma}$ and the higher-order stress $\boldsymbol{\tau}$, and in the presence of a hard inclusion, a stress concentration is

seen. What appears as a discontinuity in the shear stress, σ_{12}, for the strain gradient plasticity theory (the points labelled 'SG') is actually a high gradient at the boundary of the hard layer. The shear stress diminishes away from the boundaries; both within the embedded layer and in the matrix.

Both characteristics represented in the numerical examples: a softening band width determined by the material length scale, and the stress intensification near a hard inclusion, are hallmarks of a strain gradient theory. The fine-scale physics is represented by the multiscale model which was constructed by embedding the fine-scale strain gradient theory in the macroscopic formulation. Importantly, this was done without refining the mesh size down to the scales of the embedded layer. A uniform mesh size of 1 m was used throughout. The region Ω' was taken to be the element containing the embedded layer (of width 2×10^{-6} m) and the strain gradient plasticity theory specified as the fine-scale physics model over all of Ω'.

Microforce theories of the class mentioned in Section 1 can also be treated in this framework.

6. CONCLUSION

The treatment of fine-scale physics envisaged in this article encompasses fine-scale theories that prevail at length scales of a micron. The long-term goal of this work is to build a broad formalism by which to embed—potentially any—such theories in macromechanical continuum formulations. As seen with the treatment of the Fleck–Hutchinson strain gradient theory, and earlier work with traction-separation laws [26] some of these fine-scale models *require* a vehicle like the multiscale method proposed here to make the notion of this embedding meaningful. Others, such as microforce theories naturally incorporate such coupling between micro- and macroscale response. In such cases, the methods proposed here will serve as computational formulations to preserve the tight coupling of scales needed to realize the potential of these theories.

REFERENCES

1. Nix WD. Mechanical properties of thin films. *Metallurgical Transactions* 1989; **20A**:2217–2245.
2. De Guzman MS, Newbauer G, Flinn P, Nix WD. The role of indentation depth on measured hardness of materials. In *Materials Research Symposium Proceedings*, vol. 308, 1993; 613–618.
3. Stelmashenko NA, Walls MG, Brown LM, Milman YV. Microindentation studies on W and Mo oriented single crystals. *Acta Metallurgica et Materialia* 1993; **41**:2855–2865.
4. Ma Q, Clarke DR. Size dependent hardness in silver single crystals. *Journal of Materials Research* 1995; **10**:853–863.
5. Poole WJ. Ashby MF, Fleck NA. Microhardness of annealed and work-hardened copper polycrystals. *Scripta Metallurgica et Materialia* 1996; **34**:559–564.
6. McElhaney KW, Vlassak JJ, Nix WD. Determination of indenter tip geometry and indentation contact area for depth-sensing indentation experiments. *Journal of Materials Research* 1998; **13**:1300–1306.
7. Fleck NA, Muller GM, Ashby MF, Hutchinson JW. Strain gradient plasticity: theory and experiment. *Acta Metallurgica et Materialia* 1994; **42**:475–487.
8. Stolken JS, Evans AG. Microbend test method for measuring the plasticity length scale. *Acta Materialia* 1998; **46**:5109–5115.
9. Lloyd DJ. Particle reinforced aluminum and magnesium matrix composites. *International Materials Review* 1994; **39**:1–23.
10. Steinmann P. Views on multiplicative elastoplasticity and the continuum theory of dislocations. *International Journal of Engineering Science* 1996; **34**:1717–1735.
11. Fleck NA, Hutchinson JW. Strain gradient plasticity. *Advances in Applied Mechanics* 1997; **33**:295–361.

12. Gao H, Huang Y, Nix WD. Mechanism-based strain gradient plasticity—I. Theory. *Journal of the Mechanics and Physics of Solids* 1999; **47**:1239–1263.
13. Aifantis EC. Gradient deformation models at nano, micro, and macro scales. *Journal of Engineering Materials and Technology* (ASME) 1999; **121**:189–202.
14. Arsenlis A, Parks DM. Crystallographic aspects of geometrically-necessary and statistically-stored dislocation density. *Acta Materialia* 1999; **47**:1597–1611.
15. Acharya A, Bassani JL. Lattice incompatibility and a gradient theory of crystal plasticity. *Journal of the Mechanics and Physics of Solids* 2000; **48**:1565–1595.
16. Acharya A, Beaudoin JL. Grain-size effect in viscoplastic polycrystals at moderate strains. *Journal of the Mechanics and Physics of Solids* (ASME) 2000; **48**:2213–2230.
17. Menzel A, Steinmann P. On the continuum formulation of higher gradient plasticity for single and polycrystals. *Journal of the Mechanics and Physics of Solids* 2000; **48**:1777–1796.
18. Gurtin ME. The nature of configurational forces. *Archive for Rational Mechanics and Analysis* 1995; **131**: 67–100.
19. Maugin GA. Material forces: concepts and applications. *Applied Mechanics Reviews* (ASME) 1995; **48**:213–245.
20. Fried E, Gurtin ME. Coherent solid-state phase transitions with atomic diffusion: a thermomechanical treatment. *Journal of Statistical Physics* 1999; **95**:1361–1427.
21. Cermelli P, Sellers S. Multi-phase equilibrium of crystalline solids. *Journal of the Mechanics and Physics of Solids* 2000; **48**:765–796.
22. Gurtin ME. On the Plasticity of single crystals: free energy, microforces, plastic-strain gradients. *Journal of the Mechanics and Physics of Solids* 2000; **48**:989–1036.
23. Garikipati K, Hughes TJR. A study of strain localization in a multiple scale framework—the one dimensional problem. *Computer Methods in Applied Mechanics and Engineering* 1998; **159**:193–222.
24. Garikipati K, Hughes TJR. A variational multiscale approach to strain localization—formulation for multidimensional problems. *Computer Methods in Applied Mechanics and Engineering* 2000; **188**:39–60.
25. Garikipati K, Hughes TJR. Embedding micromechanical laws in the continuum formulation—a multiscale approach applied to discontinuous solutions. *International Journal for Computational Civil and Structural Engineering* 2000; **1**(1):64–78.
26. Garikipati K. A variational multiscale method to embed micromechanical surface laws in the macromechanical continuum formulation. *Computer Modeling in Engineering & Sciences* 2002; **3**(2):175–184.
27. Wei Y, Hutchinson JW. Steady state crack growth and work of fracture for solids characterized by strain gradient plasticity. *Journal of the Mechanics and Physics of Solids* 1997; **45**:1253–1273.
28. Fish J, Belsky V. Multigrid method for periodic heterogeneous media, part 2: convergence studies for one-dimensional case. *Computer Methods in Applied Mechanics and Engineering* 1995; **126**:17–38.
29. Zohdi TI, Oden JT, Rodin GJ. Hierarchical modeling of heterogeneous bodies. *Computer Methods in Applied Mechanics and Engineering* 1996; **138**:273–298.
30. Oden JT, Zohdi TI. Analysis and adaptive modeling of highly heterogeneous elastic structures. *Computer Methods in Applied Mechanics and Engineering* 1997; **148**:367–391.
31. Moes N, Oden JT, Kumar V, Remacle J. Simplified methods and *a posteriori* error estimation for the homogenization of representative volume elements (RVE). *Computer Methods in Applied Mechanics and Engineering* 1999; **176**:265–278.
32. Oden JT, Kumar V, Moes N. Hierarchical modeling of heterogeneous solids. *Computer Methods in Applied Mechanics and Engineering* 1999; **172**:3–25.
33. Huang Y, Gao H, Nix WD, Hutchinson JW. Mechanism-based strain gradient plasticity—II. Analysis. *Journal of the Mechanics and Physics of Solids* 2000; **48**:99–128.
34. Fleck NA, Hutchinson JW. A reformulation of strain gradient plasticity. *Journal of the Mechanics and Physics of Solids* 2001; **49**(10):2245–2271.
35. Shu JY, King WE, Fleck NA. Finite elements for materials with strain gradient effects. *International Journal for Numerical Methods in Engineering* 1999; **44**:373–391.
36. Engel G, Garikipati K, Hughes TJR, Larson MG, Mazzei L, Taylor RL. Continuous/discontinuous finite element approximations of fourth-order elliptic problems in structural and continuum mechanics with applications to thin beams and plates, and strain gradient elasticity. *Computer Methods in Applied Mechanics and Engineering* 2002; **191**(34):3669–3750.

